Arctic, Antarctic, and Alpine Research, Vol. 34, No. 1, 2002, pp. 12–19

Distribution Characteristics and Energy Balance of Ice Cliffs on Debris-covered Glaciers, Nepal Himalaya

Akiko Sakai

Graduate School of Environmental Studies, Nagoya University, c/o Hydrospheric Atmospheric Research Center, Nagoya 464-8601, Japan.
shakai@ihas.nagoya-u.ac.jp

Masayoshi Nakawo

Research Institute for Humanity and Nature, Kita-shirakawa, Sakyo-ku, Kyoto, 606-8502, Japan.

Koji Fujita

Graduate School of Environmental Studies, Nagoya University, c/o Hydrospheric Atmospheric Research Center, Nagoya 464-8601, Japan.

Abstract

The ablation amount for entire ice cliffs reaches about 20% of that at the whole debris-covered area; the ablation rate at the ice cliff mainly depends on shortwave radiation, which differs widely with the orientation of an ice cliff. Therefore, the distribution of ice cliffs in relation to their orientation was observed on a debris-covered glacier. The south-facing cliffs were small in area because they have low slope angles and tended to be covered with debris. The north-facing cliffs, on the other hand, were large in the studied area and maintain a slope angle larger than the repose angle of debris. They, therefore, are stable. Longwave radiation from the debris surface opposite the ice cliffs was larger on the lower portion of ice cliffs than on the upper portion in every azimuth. This difference in longwave radiation maintained a steep slope angle on ice cliff. Shortwave radiation was stronger at the upper portion of ice cliffs than at the lower portion due to the local shading effect, causing gentle sloping of ice cliffs. This was especially pronounced at cliffs facing to south. Therefore, the dependency of the ice cliff angle in orientation can be explained by the difference in local radiation between the upper and lower portion of the ice cliff.

Introduction

There are two types of glaciers in the Himalayas: debris-free glaciers (clean-type glacier) and debris-covered glaciers (Moribayashi and Higuchi, 1977). Almost all large valley glaciers, several kilometers in length, are covered with debris in their ablation zones. This type of glacier occupies more than 80% of the glacierized area in the Himalaya (Fujii and Higuchi, 1977). In the Nepal Himalaya, the meltwater from glaciers is a major water resource. Thus, it is important to examine the melt rate. It is relatively easy to measure the melt rate for a debris-free glacier, but it is difficult to measure it directly for a debris-covered glacier because of supraglacial debris. The melting processes of debris-covered glaciers remain unclear.

Several studies have indicated that the ice under a thick debris layer is kept from melting because of the insulating thick debris effect (e.g., Østrem, 1959; Fujii, 1977; Mattson et al., 1993). In Nepal Himalaya, many ice cliffs have been exposed on debris-covered glacier surfaces (Iwata et al., 1980). The mean melt rate at an ice cliff was found to be about 10 times that of debris-covered areas in Lirung Glacier located in the Nepal Himalaya (Sakai et al., 2000). Therefore, the total melt amount at ice cliffs reached as much as 18% of the total ablation in the whole debris-covered area, although the areal ratio of the cliffs was only 2% of the total (Sakai et al., 2000). Ignoring the ablation at the ice cliff would result in underestimating the ablation amount of the whole debris-covered area by 20%.

Ice cliffs are newly formed at times in two ways in Nepal Himalaya. The ice cliffs may expose as the result of a debris layer sliding, or the roof of the water channel in the glacier may collapse, exposing the ice cliff, as indicated by Kirkbride (1993). Sakai et al. (2000) indicated that the surface morphology could be rough and complicated by the collapse of the englacial water channel roof, which would be enlarged by warmed water at the pond. Iwata et al. (2000) indicated that the satellite image shows that a large relief area, where many hollows, ponds, and ice cliffs are distributed, tended to increase from less than 20% (in 1978) to more than 30% (in 1995) of the whole debris-covered area at Khumbu Glacier, Nepal Himalaya, during 17 yr.

The melt rate of ice cliffs depends mainly on shortwave radiation, which differs with the direction of the ice cliff. Sakai et al. (1998) found that the melt rate of an ice cliff facing southeast during the melting season was 11.1 cm d^{-1}, which was much larger than that of the northwest-facing ice cliff (7.0 cm d^{-1}) in Nepal Himalaya. If the area of an ice cliff facing northwest accounting for only 1% of the whole ablation area increases in the Lirung Glacier, Nepal Himalaya, the ablation would increase 10% of the ablation amount of the debris-covered area. However, if all the newly formed ice cliffs, which occupy 1% of the whole ablation area, face southeast, the total ablation amount would increase to 15% of the amount at the debris-covered area. The difference of ice cliff direction affects the ablation amount at the debris-covered area. So, azimuth dependence of the mechanism maintaining the ice cliff has an effect on the ablation of the debris-covered glacier.

Once formed, ice cliffs change their slope angle depending upon the amount of heat available for melting. But the process by which ice cliffs decrease or are maintained remains to be elucidated. In this paper, we first describe the orientation and distribution of ice cliffs and then discuss the orientation dependence of the ablation rate at ice cliffs.

Study Area and Methods

Field observations were carried out on the debris-covered ablation area of the Lirung Glacier in Langtang Valley (86°E, 28°N), Nepal Himalaya, 60 km north of Kathmandu, the capital city of Nepal (Fig. 1). The Lirung basin covers 13.8 km^2, and the ablation area (2.3 km^2) at the time was mostly covered with

1523-0430/02 $7.00

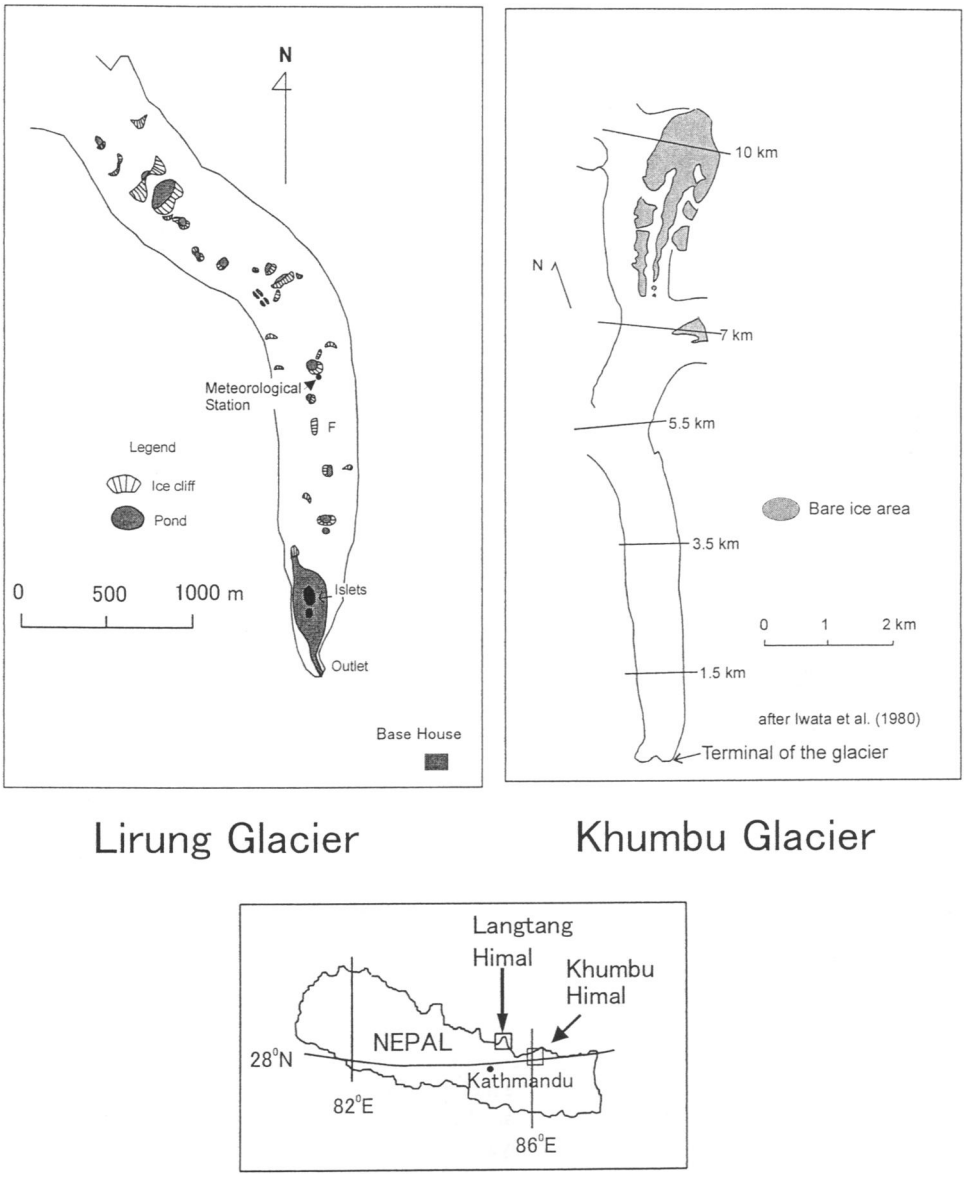

FIGURE 1. Map of the debris-covered areas in Lirung Glacier, Langtang Himal and Khumbu Glacier, Khumbu Himal.

debris. The total area of ice cliffs accounted for about 2% of the total debris-covered area in 1996 (Sakai et al., 1998).

A meteorological station was set up at the center of the debris-covered area (Fig. 1). The observed variables were air temperature, relative humidity, wind speed, debris surface temperature, incoming and outgoing solar radiation, and net radiation. These variables were measured at a 150 cm height from the debris surface at 5-min intervals for the whole observation period from 11 May to 23 October 1996, including the summer monsoon season. The details of the observation and the preliminary results were presented by Fujita et al. (1997). Debris surface temperature and incoming shortwave radiation to the ice cliff were observed at site F (Fig. 1) at 30-min intervals. A pyranometer was installed parallel to the sloped ice surface (not horizontally). The azimuth and inclination angles of the ice cliff were 290 degrees, measured clockwise from the north at around west-northwest and 50 degrees, respectively. Cloud amount was observed manually at Base House (Fig. 1) every 3 h during the daytime.

The orientation of every ice cliff (the maximum slope inclination and the azimuth of the normal direction to the cliff surface) was measured by a clinometer several times from August to October at intervals of 2 to 3 wk. The measurement was made every 10 m only along the top edge of each ice cliff. The area of the individual cliff, in the debris-covered area, was surveyed by a laser distance finder (SOKKIA SET2000) mostly in the postmonsoon season from September to October. Several ice cliffs were newly formed and some others disappeared as a result of being covered with debris during the monsoon season. The evolution of each ice cliff was observed and recorded by photographs several times during the observation period at intervals of 2 to 3 wk.

The orientation of ice cliffs of the Khumbu Glacier were analyzed using a topographical map compiled by Iwata et al. (1980). The Khumbu Glacier, a typical debris-covered glacier, is located in the Khumbu Himal, eastern Nepal Himalaya (28°N, 86°E) (Fig. 1) about 110 km east of Langtang Valley. The total area, debris-covered area and the length of the debris covered area were 19.0 km^2, 8.3 km^2 (Fujii et al., 1977) and 11 km, respectively, much larger than the Lirung Glacier. The total ice cliff area of the Khumbu Glacier was about 2.6% of the whole debris-covered area.

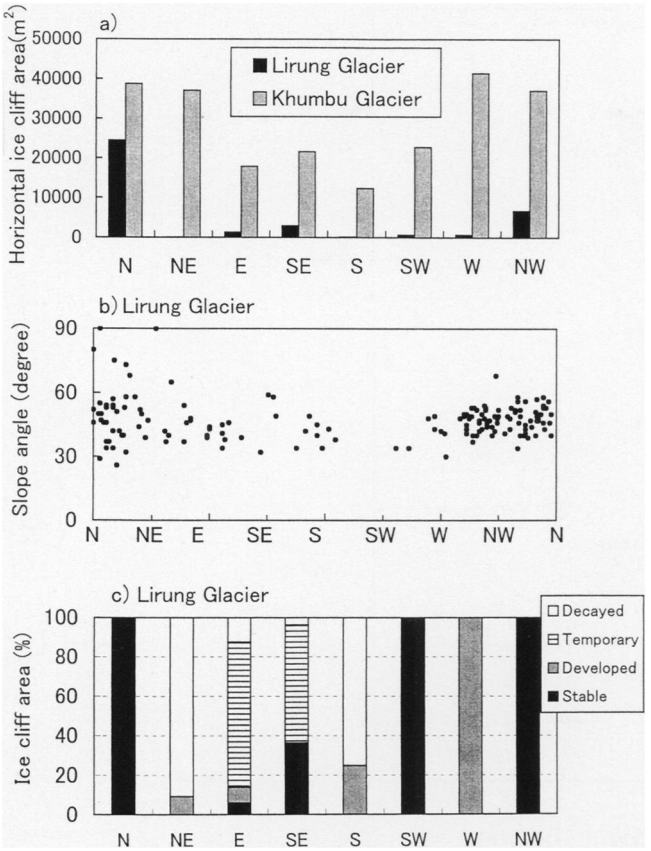

FIGURE 2. (a) Observed distribution of total horizontal area of ice cliffs divided by eight azimuths in the Lirung Glacier and the Khumbu Glacier. (b) The relation of observed inclination angle with azimuth of ice cliffs on the Lirung Glacier. (c) Percentage of four types of ice cliff area on the Lirung Glacier, projected on the horizontal plane, versus the azimuth angles which are divided into eight directions as shown in Figure 2a.

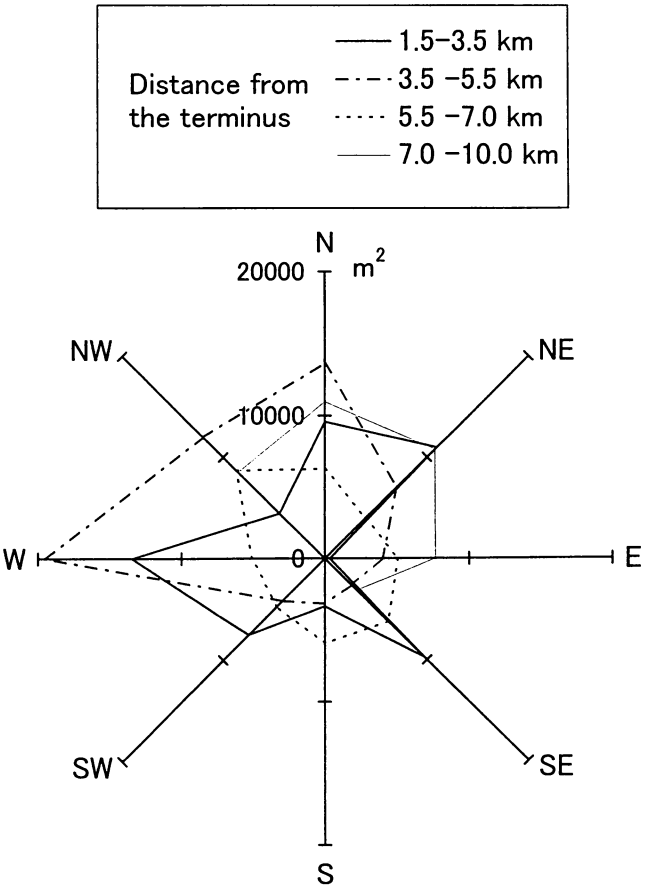

FIGURE 3. Distribution of horizontal area of ice cliffs on the Khumbu Glacier divided by four areas from the glacier terminus as shown in Figure 1.

Results

ORIENTATION OF ICE CLIFFS

Figure 2a shows the sum of the horizontal areas of ice cliffs (the sloped areas were projected on a horizontal plane) plotted in eight directions for the Lirung Glacier and the Khumbu Glacier. Ice cliffs facing north and northwest in the Lirung Glacier had large areas. Similarly, the cliff azimuth in the Khumbu Glacier was largely west and north. The area of southward-facing cliffs was small in both glaciers.

Figure 3 shows the area distribution of the orientation of ice cliffs on the Khumbu Glacier. As shown in Figure 1, the ice cliff was divided into five areas from the upper to the lower part of the ablation zone. Ice cliffs in the upper ablation zone faced in random directions, and toward the glacier terminus the direction became more and more northwesterly.

INCLINATION ANGLE OF ICE CLIFFS

The observed relation between the inclination angle and the azimuth of ice cliffs is shown in Figure 2b for the Lirung Glacier. No ice cliffs were found with inclinations of more than 90 degrees (i.e. overhanging). Most ice cliff inclinations ranged from 30 to 60 degrees, varying widely up to 90 degrees for cliffs facing northward. The average inclination angles in the southward azimuth (clockwise from east to west) were lower than for northward (clockwise form west to east) (Fig. 2b). There were no cliffs with an angle less than 30 degrees, which corresponded to the typical internal friction angle for coarse sediment (Terzaghi and Peck, 1967). The internal friction angle might depend on the size of debris and water content. The observed inclination of an ice cliff just exposed was 34 degrees. Therefore, the maximum repose angle of debris was considered between 30 and 35 degrees on the Lirung Glacier.

DEVELOPMENT AND DECAY OF ICE CLIFFS

Ice cliffs on the Lirung Glacier were classified into four types, Decayed, Temporary, Developed, and Stable, based on the field observation and intermittent photographs of the cliffs. Decayed ice cliffs are those which have become small in area, and which eventually become almost completely covered with debris in the postmonsoon season. Temporary cliffs are exposed with debris sliding only in the monsoon season and disappear when covered by debris in the postmonsoon season. Developed ice cliffs have become large in cliff area. Stable ice cliffs are those which did not change in area during the observation period in 1996. Figure 2c shows the total area of the four types of ice cliffs depending upon the azimuth angle divided into eight directions. The area ratio of Stable or Developed ice cliffs was large, when viewed clockwise from southwest to north, whereas that of Decayed or Temporary ice cliffs was large, when viewed clockwise from northeast to south. Thus, an ice cliff facing southeastward was unstable, whereas an ice cliff facing northwestward was stable.

Distribution of Radiation on Ice Cliff

Figures 2a and 2b show that the area of ice cliffs facing southward was small in total area, and the slope was generally gentle, compared with those facing northward. On the other hand, ice cliffs facing northward were large in area and rather steep in slope. Figure 2b also shows that the inclination angle of all ice cliffs was larger than 30 degrees, suggesting that the ice surface with the inclination of less than 30 degrees would be covered and buried with debris. The relatively small area of south-facing cliffs, therefore, could be the result of their rather gentle slope, which tended to be covered with debris. Ice cliffs facing northward were generally steep in slope, and could keep their ice surface exposed. Why do north-facing ice cliff surfaces have steep slopes and south-facing cliffs gentle slopes?

The debris surface showed a highly heterogeneous topography, with many mounds, ridges, valleys, and hollows. It is necessary to take into account the effect of the shadow of opposite debris slopes, and longwave radiation from adjacent debris surfaces whose temperature was much higher than that of ice cliffs (Plüss and Ohmura, 1997). Ice-cliff inclination depends on the difference in the melt rate between the upper and lower portion of the ice cliffs. If the melt rate in the upper portion of an ice cliff is larger than that in the lower portion, the ice-cliff inclination should become less steep. On the other hand, if the melt rate in the upper part is almost equal to that in the lower portion, the ice-cliff inclination should be maintained. Therefore, the differences in the shortwave and longwave radiations between the upper and lower portions were estimated.

LONGWAVE RADIATION FROM OPPOSITE SIDE OF DEBRIS SURFACE

Figure 4a shows the daily mean debris surface temperatures observed at the meteorological station and at site F. The average debris surface temperature during the observation period was 10°C, which was almost equal to the observed debris surface temperature at the meteorological station on Lirung Glacier. Figure 4b shows the diurnal fluctuation of debris surface temperature at both sites from 21 to 25 August. Those debris surface temperatures at both sites exceed 30°C during the daytime, and they were much higher than the temperature of the ice surface (melting point, 0°C). Ice cliffs receive a large amount of longwave radiation from the debris surface facing them and from the mountain range surrounding the glacier.

The overlying hemisphere was divided into two: the sky and the adjacent debris surface. It was assumed that the sky portion included the surrounding high mountains since the difference in the longwave radiation between the upper and lower portions of the ice-cliff surface was relatively smaller than that of the adjacent debris surface. Therefore, the incoming longwave radiation to an ice cliff, $LR_i\downarrow$, is expressed as follows (Marks and Dozier, 1979):

$$LR_i\downarrow = v_{sky}LR\downarrow + v_{deb}LR_d\uparrow \quad (1)$$

where,

$$v_{sky} + v_{deb} = 1 \quad (2)$$

$$LR_d\uparrow = \epsilon_d\sigma T_d^4 \quad (3)$$

where,

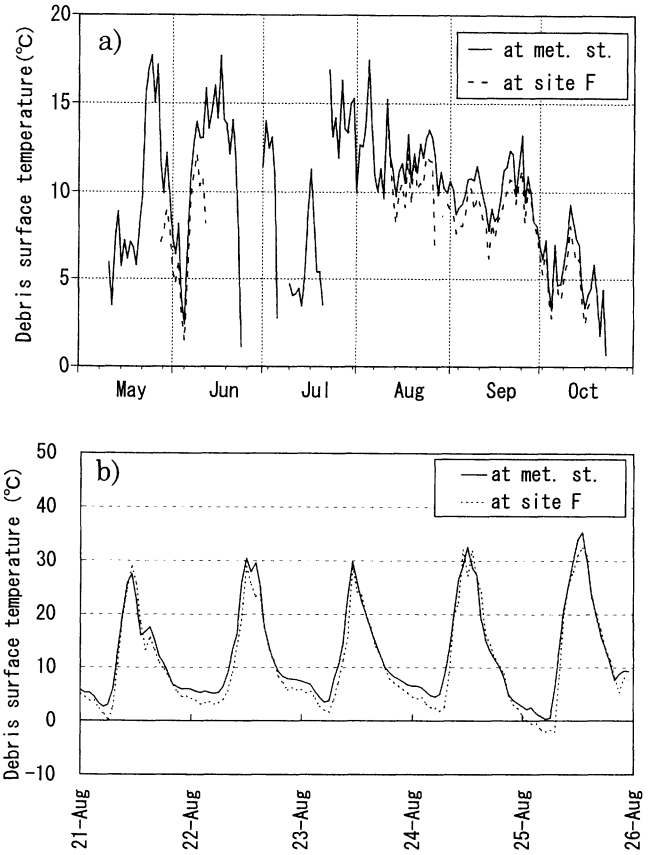

FIGURE 4. (a) Daily average debris surface temperature observed at meteorological station and site F. (b) Debris surface temperature observed at meteorological station and site F at 1-h intervals from 21 to 25 August.

$LR\downarrow$ = Longwave radiation from the sky and surrounding high mountains,
LR_d = Longwave radiation from adjacent debris surfaces,
ϵ_d = Emissivity of debris surface (=0.98) (Oke, 1987),
σ = Stefan-Boltzman constant ($=5.67 \times 10^{-8}$ W m^{-2} K^{-4})
T_d = Debris surface temperature [K]
v_{sky} = View-factor of the sky and surrounding high mountains, and
v_{deb} = View-factor of adjacent surrounding debris surface.

View-factor of the sloped ice-cliff surface was defined as shown in Figure 5a from the elevation angle, which was defined as the angle between the peak edge of debris and the horizontal surface as shown in Figure 5b. Elevation angles of the edge of the debris slope in relation to each ice cliff were measured at every 10 degrees in azimuth from a topographical map with contour lines at 10-m intervals (Aoki and Asahi, 1998). The elevation angle should be 0 degree when the plane surface is expanding, and 90 degrees if there is vertical slope in the elevation angle. The view factor may take any value between zero (minimum topographic obstruction) and one (maximum topographic obstruction). The shadowed portions in Figure 5a indicate the overlying debris surface adjacent to the ice cliff. The calculation of view factors of the sloped surface from the elevation angle data were made according to Dozier and Frew (1990). The lower portion of ice cliffs should receive more longwave radiation since the view factor of the debris surface, which has a surface temperature much higher than the sky at the lower part, is larger than in the upper portion.

There is no longwave radiation income from adjacent debris

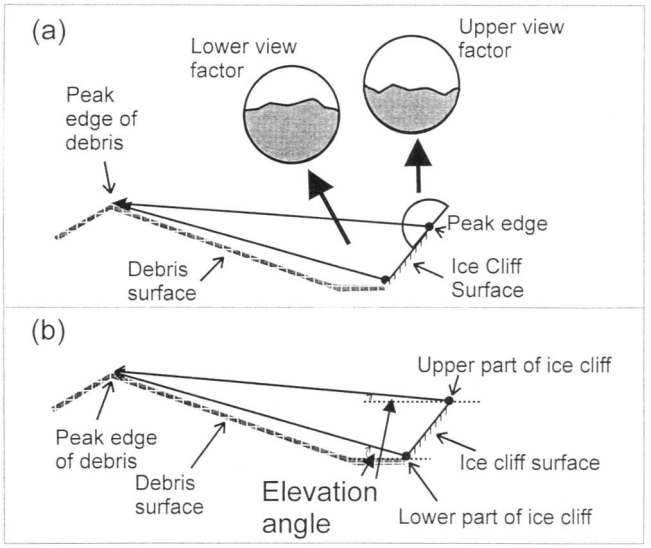

FIGURE 5. (a) Elevation angles of adjacent debris surface in relation to the upper and lower part of ice cliffs. (b) Sky-view factor for the partially obstructed, sloped ice cliff surface. Shaded part is the debris-covered slope and white part is sky.

surfaces at the meteorological station, which was set up at the peak of the cone of the debris surface (v_{deb} = 0). Therefore, the observed longwave radiation at the meteorological station is equal to $LR\downarrow$ in equation (1). Net radiation, downward and upward shortwave radiations, and surface temperature were observed at the meteorological station. Downward longwave radiation at the meteorological station, where the glacier surface was covered with a thick debris layer, was estimated using the following equation:

$$LR\downarrow = NR - SR\downarrow + SR\uparrow + \epsilon_d \sigma T_s^4 \quad (4)$$

where,

NR = Net radiation [W m^{-2}]
T_s = Surface temperature [K]
$SR\downarrow$ = Downward shortwave radiation, and
$SR\uparrow$ = Upward shortwave radiation.

Figure 6 shows the calculated downward longwave radiation at the meteorological station, $LR\downarrow$, and the upward longwave radiation at sites of meteorological station and the site F, $LR_d\uparrow$, calculated from equations (2) and (4), respectively. The calculated mean longwave radiation from the sky and surrounding high mountains at the meteorological station and the longwave radiation from the debris surface were 284 W m^{-2} and 357 W m^{-2}, respectively, from May to October. The amount of longwave radiation from the sky was relatively small in May and October compared to the monsoon season, from June to September.

View factors of adjacent debris surfaces at the upper and lower part of the ice cliff averaged 0.28 and 0.35, respectively, for whole ice cliffs on the Lirung Glacier. In its lower part, an ice cliff could receive more longwave radiation since the view factor of the debris surface was larger than that of the upper part. The monthly mean values obtained by subtracting the incoming longwave radiation at the upper part of the ice cliff from that of the lower part are shown in Figure 7. Incoming longwave radiation to the lower portion of an ice cliff was about 4 W m^{-2} more than that to the upper portion during the monsoon season and about 7 W m^{-2} during the pre- and postmonsoon season.

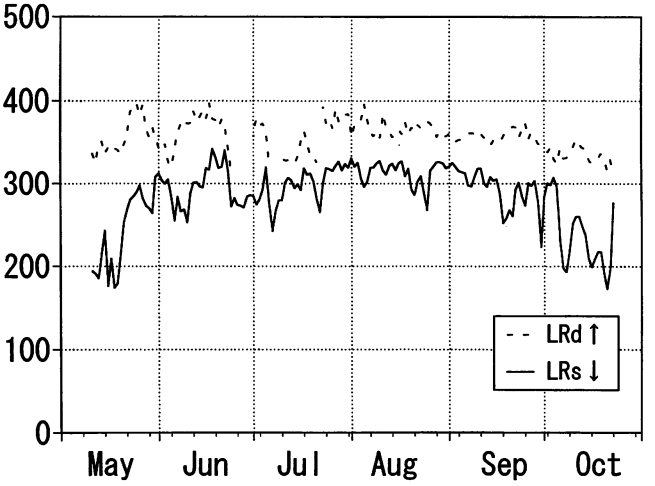

FIGURE 6. Daily average calculated longwave radiation from the sky, $LR_s\downarrow$, and debris surface, $LR_d\uparrow$.

The difference in longwave radiation between the upper and lower portions made for a steep inclination of ice cliffs.

The debris surface temperature depended on the debris thickness (Rana, 1997), which varied from place to place. The difference was about 15°C according to the satellite (TM) data at 1000 hours in May. In particular, the surface temperature of south-facing debris surfaces, which were facing the north-facing cliffs, would be higher than those of the north-facing debris, since the former received more sunshine than the latter. The north-facing ice cliffs, therefore, might receive more longwave radiation than the south facing-ice cliffs, and may have become steep more rapidly than the south-facing cliffs.

LOCAL SHADING EFFECT

The global solar radiation, S_g, on a given slope for a slope unit area was composed of direct shortwave radiation, S_d, and diffuse shortwave radiation, S_f, as follows (Garnier and Ohmura, 1968):

$$S_g = S_d \cos(X \hat{} A) + S_f \quad (5)$$

where,

X = a unit coordinate vector normal to the slope and pointing away from the ground,
A = a unit coordinate vector expressing the position away from the ground, and
^ = a symbol denoting the angle between X and A.

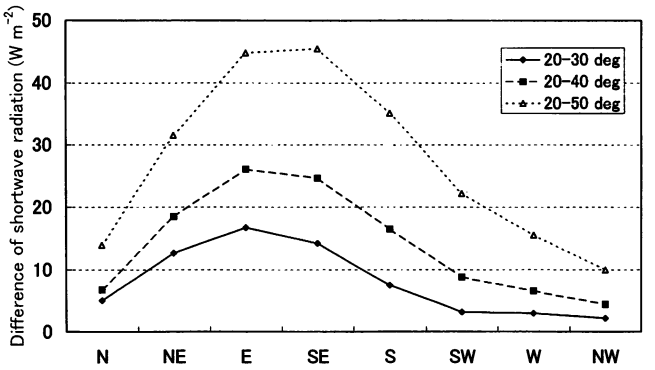

FIGURE 7. Mean subtractions of incoming shortwave radiation in upper portion from lower portion of ice cliff in eight azimuths from May to October.

Diffuse shortwave radiation was scattered, came from diverse sources, and depended on many factors including the turbidity of the atmosphere, and surrounding terrain (Duguay, 1993).

Sakai et al. (1998) found that the major heat source for ice cliff melting was the shortwave radiation income. They estimated the amount of incoming direct shortwave radiation for slopes with various azimuths and slope angles of the entire observation period, taking into account intervening cloud cover. During the monsoon season, the weather was cloudy almost every afternoon in the Nepal Himalaya. There must be much diffuse shortwave radiation coming from clouds. Sakai et al. (1998), however, neglected the diffuse shortwave radiation in order to estimate the incoming shortwave radiation to the sloped ice cliff.

Direct shortwave radiation has directivity and depends on the cloud distribution in the sky, where the clouds keep out the sunlight. The probability of the sun being covered with clouds would depend on the amount of cloud cover. If the assumption is made that the diffuse radiation and direct solar radiation are uniform on each cloudy and clear portion of the sky, the diffuse solar radiation is composed of incoming diffuse solar radiation from the clear portion and cloudy portion of the sky. Moreover, the global solar radiation is also composed of incoming global shortwave radiation from the clear and cloudy portions of the sky as follows:

$$S_f = (1 - C)S_{fc} + CS_{fo} \tag{6}$$

$$S_g = (1 - C)S_{gc} + CS_{go} \tag{7}$$

where,

C = Cloud amount (0–1)
S_{fc} = Diffuse shortwave radiation on clear day,
S_{fo} = Diffuse shortwave radiation when the sky is completely overcast,
S_{gc} = Global shortwave radiation on clear day, and
S_{go} = Global shortwave radiation when the sky is completely overcast.

The ratio of the direct shortwave radiation to the global shortwave radiation was expressed as follows from equations (5), (6), and (7):

$$\frac{S_d}{S_g} = 1 - \frac{S_f}{S_g} = 1 - \frac{(1 - C)S_{fc} + CS_{fo}}{(1 - C)S_{gc} + CS_{go}}. \tag{8}$$

With the observed or estimated data of C, S_{fc}, S_{fo}, S_{gc}, S_{go}, and S_g, the direct shortwave radiation can be estimated from equation (8) above.

There is no direct shortwave radiation on overcast days (Nunez, 1980). Therefore, we considered the solar radiation, S_{go}, to be equal to the diffuse shortwave radiation, S_{fo}, for an overcast day (S_{go} [$=S_{fo}$]) and a clear day (S_{gc}) each month from among the cloud amount data obtained manually at the Base House. A sensor for shortwave radiation was installed parallel to the sloped ice cliff at site F. Diffuse radiation including diffuse shortwave radiation from surrounding terrain was observed in the morning since the sensor was oriented northwest. The observed diffuse radiation on a clear day was 16% of the incoming radiation in average. The value of 16% was used in the present study since diffuse radiation (S_{fc}/S_{gc} = 0.16) was observed.

Figure 8 shows the mean monthly diurnal change in cloud amount observed at 3-h intervals (0600, 0900, 1200, 1500, 1800). The cloud amount had an increasing tendency from morning to evening during the observation period. The weather was

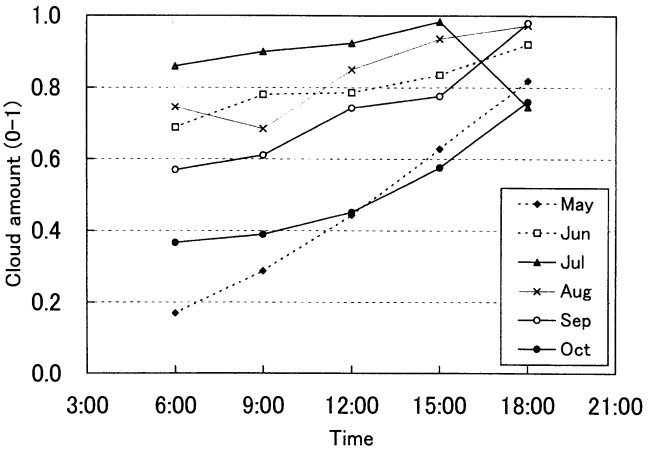

FIGURE 8. Monthly average diurnal change of cloud percent coverage observed at 3-h intervals.

relatively fine on mornings with small amounts of precipitation and strong solar radiation (Sakai et al., 1998). From noon, however, it was cloudy or rainy, in association with low solar radiation. The maximum solar radiation was found in the diurnal change at 1000 (Sakai et al., 1998), when the cloud cover was relatively small for the radiation averaged for the observation period.

Ice cliffs were surrounded by the adjacent debris surfaces of the glacier and high mountains. The elevation angles of the surrounding high mountains in relation to the upper and lower part of ice cliffs showed no difference since the high mountains were located far away from the ice cliffs compared to the debris surfaces. Elevation angles of surrounding high mountains observed at the meteorological station were distributed between 10 to 35 degrees with an average of about 20 degrees. The mean elevation angle of adjacent debris surface in relation to the upper part of ice cliffs was 6 degrees at the Lirung Glacier with a maximum of 20 degrees. The elevation angle of adjacent debris surface in relation to the upper part of the ice cliffs was smaller than the elevation angle of such surfaces in the surrounding mountains. Thus, the shading effect on the upper part of the ice cliff depends on the surrounding high mountains, not the adjacent debris surface. The elevation angle of adjacent debris surface in relation to the lower part of ice cliffs ranges from 20 to 50 degrees on the Lirung Glacier.

The difference of incoming direct shortwave radiation between the upper and lower part of the ice cliffs was calculated where the elevation angle of the shaded lower part of the ice cliff is kept at 20 degrees. There was no direct shortwave radiation, and only diffuse radiation resulted when the sun was shaded by surrounding terrain.

The diurnal variation of monthly average direct shortwave radiation at 1-h intervals can be calculated from equation (8) The observed cloud amount and the shortwave radiation on cloudy days measured at 3-h intervals were interpolated as linear change. The incoming direct shortwave radiation to ice cliffs in each direction was converted from direct shortwave radiation to horizontal surface.

Figure 7 shows the mean differences in incoming direct shortwave radiation when the upper portion of an ice cliff was shaded at an elevation angle of 30, 40, and 50 degrees, respectively, during the observation period. The ice cliff azimuth is shown for eight different directions, respectively. Those differences increased with the increase in the difference of the elevation at the upper and lower part. Slopes facing northeast to

southeast had the largest differences in shortwave radiation, whereas those facing west to north had relatively small differences, due to cloud cover. This was mainly because the weather was fine mornings and the sun shone on slopes facing east; it was cloudy and rainy afternoons, and the slopes facing west received relatively little direct solar radiation (Sakai et al., 1998).

The shade of the adjacent debris surface served to decrease the melt rate at the lower portions of cliffs, while the higher portions were more affected. This caused the slope to become less steep, especially at cliffs facing northeast to southeast. In contrast, this shading effect would be much less around northwest-facing cliffs since the upper portion of the ice cliffs received less direct shortwave radiation than the lower portion.

Discussion

The differences in longwave and shortwave radiations in the upper and lower parts of ice cliffs facing clockwise from west to north were on the same order of about 5 W m^{-2}. Therefore, the melt rate at the upper and lower part was almost the same at the ice cliffs facing west to north. Moreover, the slope of the ice cliffs remains steep. Therefore, ice cliffs facing northwest have continous ice exposure.

On the other hand, with ice cliffs facing from northeast to south, the shading effect, which prevented melting at the lower part, was larger than the effect of the longwave radiation from the debris surface. Therefore, the ice cliffs facing from northeast to south tended to have a gentle slope if there was some adjacent debris surface with a high elevation angle. These local differences in radiations can explain differences we observed between north-facing and south-facing ice cliff distribution at the Khumbu Glacier and Lirung Glacier in Figure 2. On the other hand, the area and the inclination of ice cliff facing west were almost the same as those of ice cliff facing east at the Lirung glacier as shown in Figures 2a and 2b. However, an ice cliff facing west should have a larger area and steeper slope than a cliff facing east according to the local radiation difference. More investigations must be made on the longwave radiation from around mountains, and the relation between formation of an ice cliff and the flow dynamics of a glacier. Furthermore, the average incoming turbulent heat (sensible and latent) was 99 W m^{-2} from May to October. Both sensible and latent heat could affect the change in slope angle, although such kinds of heat were relatively smaller in the proportion the incoming shortwave and longwave radiation. In the Nepal Himalaya, the valley wind develops in the daytime during the monsoon season (Ageta, 1976). The wind was observed to blow from the south on both the Lirung Glacier and the Khumbu Glacier, which flow southward. The sensible and latent heat would contribute to faster melting at the upper part of ice cliffs facing windward than at the lower part.

The upper portion of ice cliffs facing south received more shortwave radiation. Therefore, the ice cliffs facing south tended to have gentle slopes if there was some adjacent debris surface with a high elevation angle. The average inclination of ice cliffs facing south, i.e., the Decayed type, was observed to be 40 degrees. At the end of the melting season the inclination conceivably became 34 degrees, which was the internal friction angle of debris when the ice cliffs were covered by it. If the ice cliff height is 5 m with a 40-degree slope, it takes a melting season of about 370 d to change the inclination 34 degrees when the difference of incoming radiation at the upper and lower part is 10 W m^{-2}, about 180 d when the difference is 20 W m^{-2}, and about 120 d when the difference is 30 W m^{-2}. Therefore, even if the hollows surrounded by ice cliffs appear on the upper part of debris-covered glacier surfaces, the ice cliffs facing south would disappear and the those facing north would survive after a few years while the glacier ice gradually flows down to the terminus. The above mentioned calculation of time for the disappearance of ice cliff facing south accounts for that the distribution of ice cliff orientations tend to be northwest from upper to lower at the Khumbu Glacier, because the ice cliffs would be formed in the at upper and middle portions of a debris-covered area as shown in Figure 3. Ice cliffs are formed at the edge of a hollow created by the collapse of the roof of a water channel in the glacier (Kirkbride, 1993). Therefore, a hollow with its entire edge surrounded by ice cliffs, would be newly formed, whereas hollows with ice cliffs facing only north would be formed more than a few years earlier. The process of the hollow formation should be clarified to evaluate the ablation amount at a debris-covered glacier taking into account the ablation at ice cliffs.

Conclusion

Field observation showed that north-facing cliffs were large in total area, steep in slope angle and stable. On the other hand, south-facing cliffs were small in area, gentle in slope and tended to disappear.

More longwave radiation from the debris surface reaches the lower portion of the ice cliff than the upper portion. The difference in longwave radiation makes the ice cliff steep. The direct incoming shortwave radiation, the major heat for melting ice cliffs, was found to be greater in the upper part of the ice cliff than the lower one, especially in the southerly direction. Therefore, ice cliffs facing south tend to disappear because their angle recedes below the angle of repose of the debris, and the ice cliffs become debris-covered, whereas the north-facing ice cliffs maintain an angle greater than the angle of repose, and the ice cliff would presumably continue to be exposed.

Azimuth dependence of the distribution characteristics of ice cliffs could be explained by taking into account the local shading by surrounding ridges and longwave radiation from adjacent debris surfaces. Also, other factors at work include turbulent heat and the relation between formation of ice cliff and dynamic flow.

The mechanisms by which an ice cliff is maintained or disappears were clarified. However, the changes in surface morphology should be observed at an interval of several years, and the initial formation process of ice cliffs must be investigated to permit estimation of the ablation amount of debris-covered glaciers including the melt amount at ice cliffs.

Acknowledgments

We would like to express our thanks to the Department of Hydrology and Meteorology, Ministry of Water Resources, His Majesty's Government of Nepal. We also thank Dr. T. Aoki and Dr. S. Ishikawa for valuable discussions and comments on this work. We are also grateful to all of the members of the Project for their kind support in the field. The expenses for the field research and data analyses were supported by a Grant-in-Aid for Scientific Research (Project No. 06041051, No. 09490018, No. 13373006, and No. 13573004) from the Ministry of Education, Science, Sports and Culture, Japanese Government and JSPS Research Fellowships for Young Scientists.

References Cited

Ageta, Y., 1976: Characteristics of precipitation during monsoon season in Khumbu Himal. *Seppyo,* 38 (Special Issue): 84–88.

Aoki, K. and Asahi, K., 1998: Topographical map of the ablation area of the Lirung Glacier in the Langtang Valley, Nepal Himalaya. *Bulletin of Glacier Research,* 16: 19–31.

Dozier, J. and Frew, J., 1990: Rapid calculation of terrain parameters for radiation modeling from digital elevation data. *IEEE Transactions on Geoscience and Remote Sensing,* 28(5): 963–969.

Duguay, C. R., 1993: Radiation modeling in mountainous terrain reviews and status. *Mountain Research and Development,* 13: 339–357.

Fujii, Y., 1977: Field experiment on glacier ablation under a layer of debris cover. *Seppyo,* 39 (Special Issue): 20–21.

Fujii, Y. and Higuchi, K., 1977: Statistical analyses of the forms of the glaciers in the Khumbu Himal. *Seppyo,* 39 (Special Issue): 7–14.

Fujita, K., Sakai, A., and Chhetri, T. B., 1997: Meteorological observation in Langtang Valley, Nepal Himalayas, 1996. *Bulletin of Glacier Research,* 15: 71–78.

Garnier, B. J. and Ohmura, A., 1968: A method of calculating the direct shortwave radiation income of slopes. *Journal of Applied Meteorology,* 7: 796–800.

Iwata, S., Watanabe, O., and Fushimi, H., 1980: Surface morphology in the ablation area of the Khumbu Glacier. *Seppyo,* 41 (Special Issue): 9–17.

Iwata, S., Aoki, T., Kadota, T., Seko, K., and Yamaguchi, S., 2000: Morphological evolution of the debris cover on Khumbu Glacier, Nepal, between 1978 and 1995. *In* Nakawo, M., et al. (eds.), *Debris-Covered Glaciers*: Proceedings of an international workshop at the University Washington in Seattle. *IAHS Publication,* 264: 3–11.

Kirkbride, M. P., 1993: The temporal significance of transitions from melting to calving termini at glaciers in the central Southern Alps of New Zealand. *The Holocene,* 3: 232–240.

Mattson, L. E., Gardner, J. S., and Young, G. J., 1993: Ablation on debris covered glaciers: an example from the Rakhiot Glacier, Punjab, Himalaya. *In* Jones, H. G., et al. (eds.), *Snow and Glacier Hydrology: Proceedings of Yokohama Symposia. IAHS Publication,* 218: 289–296.

Marks, D. and Dozier, J., 1979: A clear-sky longwave radiation model for remote alpine areas. *Archive for Meteorology, Geophysics, and Bioclimatology,* Ser. B. 27: 159–178.

Moribayashi, S. and Higuchi, K., 1977: Characteristics of glaciers in the Khumbu region and their recent variations. *Seppyo,* 39 (Special Issue): 3–6.

Nunez, M., 1980: The calculation of solar and net radiation in mountain terrain. *Journal of Biogeography,* 7: 173–186.

Oke, T. R., 1987: *Boundary Layer Climates.* 2nd. ed. London: Routledge. 435 pp.

Østrem, G., 1959: Ice melting under a thin layer of moraine and the existence of ice cores in moraine ridges. *Geografiska Annaler,* 41: 228–230.

Plüss, C. and Ohmura, A., 1997: Longwave radiation on snow-covered mountainous surfaces. *Journal of Applied Meteorology,* 36: 818–824.

Rana, B., 1997: Study on glacier ablation under debris-cover for runoff modeling of a river basin in Langtang Valley, Nepal Himalaya. Ph.D. thesis, Nagoya University. 157 pp.

Sakai, A., Nakawo, M., and Fujita, K., 1998: Melt rate of ice cliffs on the Lirung Glacier, Nepal Himalayas, 1996. *Bulletin of Glacier Research,* 16: 57–66.

Sakai, A., Takeuchi, N., Fujita, K., and Nakawo, M., 2000: Role of supraglacial pond in the ablation process of a debris-covered glacier in the Nepal Himalayas. *In* Nakawo, M., et al. (eds.), *Debris-Covered Glaciers:* Proceeding of an International Workshop at the University Washington in Seattle. *IAHS Publication,* 264: 119–130.

Terzaghi, K. and Peck, R. B., 1967: *Soil Mechanics in Engineering Practice.* 2nd ed. New York: John Wiley. 729 pp.

Ms submitted March 2000
Revised ms submitted March 2001